Earth and Planetary Science Letters 620 (2023) 118336

Contents lists available at ScienceDirect

Earth and Planetary Science Letters

journal homepage: www.elsevier.com/locate/epsl

Constraining the onset and environmental setting of metazoan biomineralization: The Ediacaran Nama Group of the Tsaus Mountains, Namibia

Fred T. Bowyer [a,*], Collen-Issia Uahengo [b,*], Kavevaza Kaputuaza [b], Junias Ndeunyema [b], Mariana Yilales [a], Ruaridh D. Alexander [a], Andrew Curtis [a], Rachel A. Wood [a]

[a] School of GeoSciences, University of Edinburgh, James Hutton Road, Edinburgh EH9 3FE, UK
[b] Department of Geosciences, University of Namibia, Keetmanshoop, Namibia

ARTICLE INFO

Article history:
Received 28 March 2023
Received in revised form 7 July 2023
Accepted 25 July 2023
Available online 17 August 2023
Editor: L. Coogan

Keywords:
Ediacaran
Nama Group
carbon isotopes
biomineralization
Namibia
stratigraphy

ABSTRACT

The advent of animal (metazoan) biomineralization marks a fundamental transition in Earth's history, facilitating the diversification of novel body plans as well as the biological control of carbonate sediment production, resulting in a permanent restructuring of the global carbon cycle. The oldest known skeletal metazoans, the tubular 'cloudinids' e.g., *Cloudina*, appeared during the terminal Ediacaran of the Nama Group, Namibia, but precisely when, where, and why metazoans first acquired the ability to biomineralize and their timing relative to the regional $\delta^{13}C_{carb}$ profile is undocumented. Assessing possible environmental triggers for this key event therefore requires accurate constraint of the age, paleoenvironmental setting and the geochemical context of the earliest cloudinids.

Here we present new stratigraphic, sedimentological, and geochemical ($\delta^{13}C_{carb}$ and $\delta^{18}O_{carb}$) data from the oldest strata (Dabis Formation) of the Nama Group from the Witputs Sub-basin, exposed in the Tsaus Mountains of the Tsau Khaeb National Park (formerly Sperrgebiet). This constrains the oldest confirmed occurrence of *Cloudina* to limestones of the lower Kliphoek Member, ca. 551–550 Ma, that were deposited laterally-equivalent to the more proximal fossiliferous Kliphoek quartzite. These limestones have dominantly negative $\delta^{13}C_{carb}$ values that immediately precede recovery from the basal Nama negative $\delta^{13}C_{carb}$ excursion (BANE), and were deposited in shallow waters after a transition from semi-restricted, evaporitive-dolomitic to open marine carbonate settings. Regional correlation shows that *Cloudina* first appeared during an interval of dominantly low oxygen and unstable, regional marine redox conditions. We conclude that data do not support a long-term shift towards more stable, oxygenated conditions as a driver for the first appearance of skeletonization in metazoans, but do suggest that open marine carbonate settings with high carbonate supersaturation were required to support the calcifying *Cloudina*. In the Nama Group, the appearance of *Cloudina* also notably coincided with a major sea level lowstand, which we hypothesise may have enabled oxygenation of these more distal settings. Such an expansion of shallow marine oxygen may therefore have provided an evolutionary driver for innovations that were not metabolically costly, such as the onset of *Cloudina* biomineralization.

1. Introduction

The ability of animals to biomineralize hard parts (skeletons) evolved independently multiple times, supporting the diverse functional benefits of co-opting minerals despite a metabolic cost (Lowenstam and Margulis, 1980; Knoll, 2003; Gilbert et al., 2019, 2022). Biomineralization facilitated the diversification of many new animal body plans and ecologies, particularly during the Ediacaran-Cambrian Radiation, and enabled the increasing biological control of carbonate sediment production that resulted in a complex and protracted restructuring of the global carbon cycle that persisted throughout the Phanerozoic. Protection from bilaterian predation has been evoked as a selective force to explain the first appearance of hard parts in metazoans, but skeletons would also have

* Corresponding authors.
E-mail addresses: fred.bowyer@ed.ac.uk (F.T. Bowyer), cuahengo@unam.na (C.-I. Uahengo).

https://doi.org/10.1016/j.epsl.2023.118336

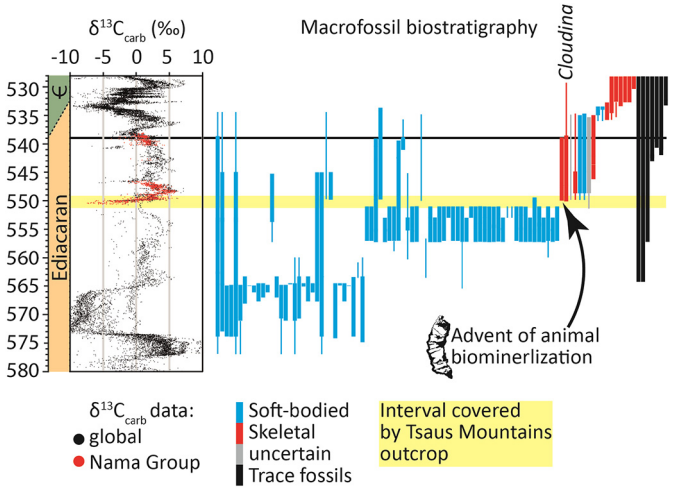

Fig. 1. Summarized fossil occurrence information from Boag et al. (2016) and Muscente et al. (2019) time calibrated relative to chemostratigraphic and radiometric age framework. $\delta^{13}C_{carb}$ age framework consistent with models C-F of Bowyer et al. (2022, 2023) and references therein, updated with new radiometric data and revised lower Cambrian calibration after Nelson et al. (2023). Line thicknesses for fossil ranges represent confidence in calibration, not relative abundance. Full, expanded figure (Fig. S1) and alternative chemostratigraphic age models that directly calibrate fossil occurrences (Table S1), in addition to full references, are provided in the Supplementary Information.

enhanced biomechanical strength as well as facilitating diverse cellular responses to changing marine chemistry, including Mg/Ca and oxygen concentrations (e.g., Degens et al., 1985; Vermeij, 1990; Knoll, 2003; Bengtson, 2004; Cohen, 2005; Wood et al., 2017).

The oldest skeletal animals, e.g., the tubular *Cloudina* and other cloudinids, have been suggested to appear ca. 551–550 Ma during the terminal Ediacaran of the Nama Group, Namibia, and then rapidly became globally widespread, persisting until ≤538 Ma (Figs. 1, S1; Germs, 1972; Zhuravlev et al., 2012; Yang et al., 2016; Nelson et al., 2022, 2023; Topper et al., 2022; Bowyer et al., 2023). But precisely when and where *Cloudina* first appeared in the Nama Group succession remains disputed, as the location of this occurrence has not been confirmed and its position relative to the regional $\delta^{13}C_{carb}$ profile is undocumented (Germs, 1983; Wood et al., 2015; Bowyer et al., 2022). *Cloudina* is found almost exclusively from carbonate settings where seawater was strongly oversaturated with respect to calcium carbonate, suggesting a limited capacity to modulate internal fluids, but the degree to which the depositional environment and early diagenesis controlled the calcification of *Cloudina* is debated (Yang et al., 2020; Shore and Wood, 2021). While the thickness of individual organic-rich laminae and the presence of internal, inter-laminar, acicular aragonitic 'cements' appear widespread, suggesting biological control, the relative thickness of the tube wall may have been environmentally controlled and there is no discernable microstructural organisation of the skeleton (Shore and Wood, 2021). In sum, there is no evidence for strong biological control of biomineralization in *Cloudina*. Resolving the trigger for this fundamental evolutionary first appearance requires a fully integrated analysis of the terminal Ediacaran chronostratigraphic, paleontological and geochemical record.

Current chronostratigraphic schemes resolve three broadly successive biotic assemblages during the latter half of the Ediacaran (ca. 576 to ≤538 Ma); the Avalon, White Sea and Nama (Figs. 1, S1, Table S1; Waggoner, 2003; Grazhdankin, 2004; Chen et al., 2014; Boag et al., 2016; Xiao et al., 2020; Yang et al., 2021; Bowyer et al., 2022; Nelson et al., 2023). Whilst the Avalon and White Sea assemblages were dominated by a variety of soft-bodied morphogroups, the Nama assemblage ca. 551 to ≤538 Ma is distinguished by the appearance and diversification of numerous skeletal and soft-bodied tubular animals, and an increase in ichnofossil diversity and bioturbation intensity (Figs. 1, S1, Table S1; Wood et al., 2023; Germs, 1972; Smith et al., 2017; Cribb et al., 2019; Muscente et al., 2019; Schiffbauer et al., 2020). This interval of evolutionary innovation occurred in the wake of a significant decline in the diversity of the soft-bodied White Sea assemblage, proposed to represent the first major animal extinction in the fossil record (Figs. 1, S1, Table S1; Darroch et al., 2018; Evans et al., 2022). However, the precise dynamics of biotic extinction and innovation across this interval are notoriously masked by a paucity of carbonate and siliciclastic depositional environments that record both calcifying and soft-bodied metazoan habitats, respectively.

The Nama Group of southern Namibia and northwest South Africa is one of the most important successions for the calibration of terminal Ediacaran to lower Cambrian chronostratigraphy (Figs. 2, S2, S3; Kaufman et al., 1991; Grotzinger et al., 1995; Saylor et al., 1995, 1998; Bowring et al., 2007; Wood et al., 2015; Linnemann et al., 2019; Nelson et al., 2022). Here, mixed carbonate and siliciclastic deposits of the lower Kuibis Subgroup stratigraphically underlie an ash bed dated at 547.36 ± 0.23 Ma (Bowring et al., 2007). Carbonates of the lower Kuibis Subgroup record recovery from a negative $\delta^{13}C_{carb}$ excursion (BANE; Figs. 2B, S3) that appears to correlate with $\delta^{13}C_{carb}$ trends in the lower Tamengo Formation, Brazil, and the Dengying Formation, South China, thereby provisionally bracketing onset of Nama Group deposition to between 555.18 ± 0.3 Ma and 550.1 ± 0.6 Ma (Figs. 1, S1; Saylor et al., 1998; Boggiani et al., 2010; Wood et al., 2015; Parry et al., 2017; Yang et al., 2021; Bowyer et al., 2022). The lowermost Nama Group therefore occupies an interval that may overlap with, or immediately postdate the transition between the White Sea and Nama assemblage biozones, as well as recording the oldest occurrence of animal biomineralization (Figs. 1, S1; Germs, 1972; Yang et al., 2021).

Here we document a new study area that hosts some of the oldest strata of the Dabis Formation of the Nama Group: the Tsaus Mountains of the Tsau Khaeb National Park. These observations constitute the first systematic description of the Tsaus Mountains in the context of Nama Group stratigraphy and paleontology. We combine our new data with published information from neighboring sections to reconstruct the regional depositional environment, $\delta^{13}C_{carb}$ chemostratigraphy, stratal stacking patterns, and paleontological record of the Kuibis Subgroup of the Witputs Sub-basin. In so doing, we constrain the relative timing and regional environmental context of the earliest Nama biotic assemblage and onset of metazoan biomineralization.

2. Geological background

The Nama Group of southern Namibia comprises a fluvial-deltaic to shallow marine mixed carbonate-siliciclastic succession subdivided into the Ediacaran Kuibis Subgroup, Ediacaran-Cambrian Schwarzrand Subgroup, and lower Cambrian Fish River Subgroup (Germs, 1983). Strata of the Kuibis and Schwarzrand subgroups outcrop over >40,000 km^2 in southern Namibia and northwest South Africa (Figs. 2A, S2), and record deposition within a series of sub-basins that developed along the western periphery of the Kalahari Craton in response to cratonic convergence and flexure associated with the Damara and Gariep orogenies during the assembly of Gondwana (Germs, 1983; Germs and Gresse, 1991). These include the northern 'Zaris' and southern 'Witputs' sub-basins (Fig. 2A). Section thicknesses in the Zaris and Witputs sub-basins increase to the north/northwest and southwest, respectively, reflecting increasing accommodation space with distance from the Kalahari Craton and an intervening paleobathymetric high, the 'Osis Arch' (Fig. 2A; Germs, 1974,

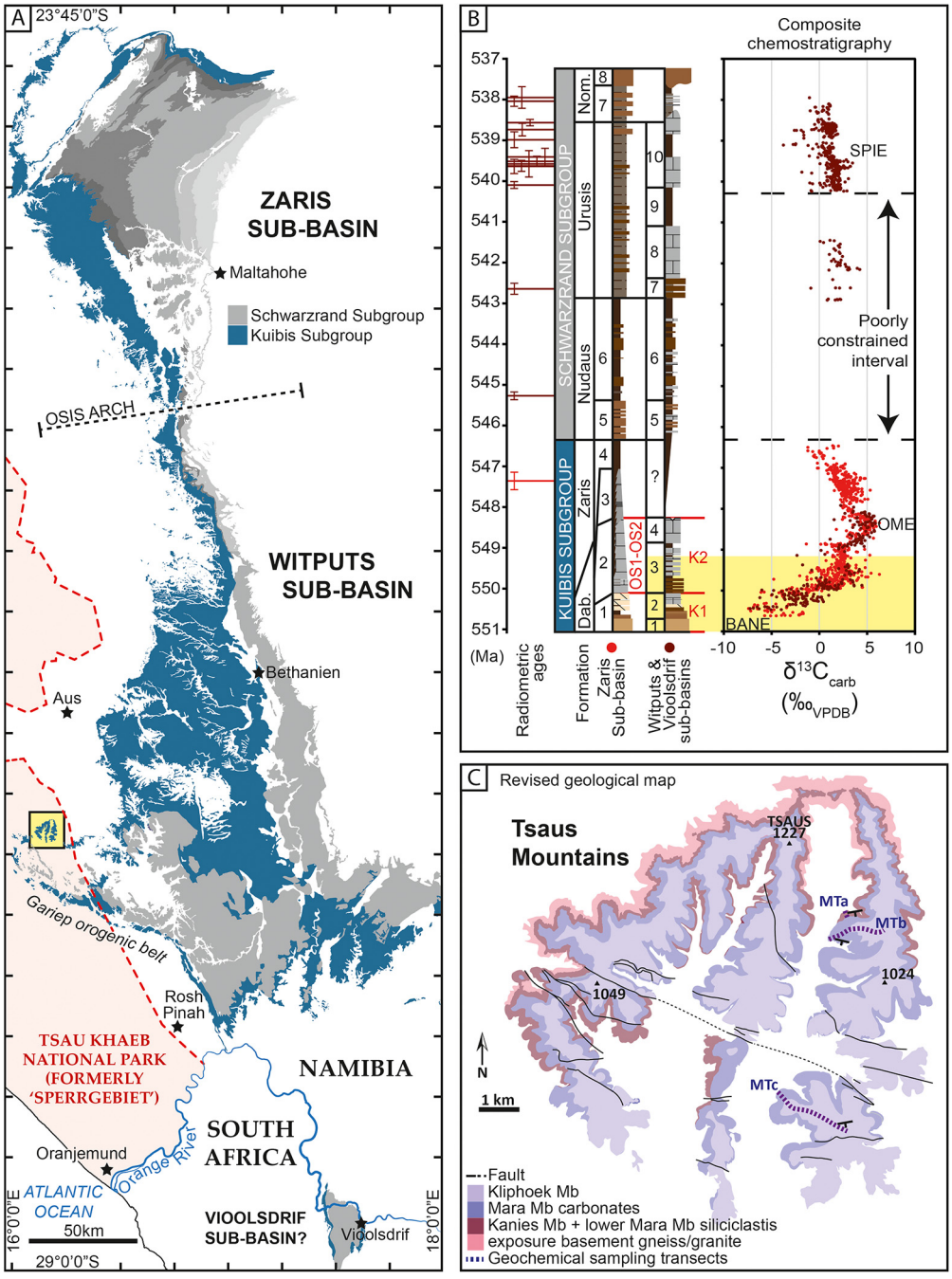

Fig. 2. (A) Geological map of the Nama Group showing position of the Tsaus Mountains. Map drafted using 1:250,000 maps of Ai-Ais (Sheet 2716, 2010), Bethanien (Sheet 2616, 1999), Gibeon (Sheet 2516, 2000), Mariental (Sheet 2416, 2017), and Rehoboth (Sheet 2316, 2006), Geological Survey of Namibia, Ministry of Mines and Energy, and map of Neint Nababeep Plateau after Nelson et al. (2022). (B) Updated and summarized lithostratigraphic and chemostratigraphic composite of the Nama Group succession, calibrated using available radiometric constraints (Bowring et al., 2007; Linnemann et al., 2019; Nelson et al., 2022). Chemostratigraphic data are colored by sub-basin. The interval corresponding to exposure in the Tsaus Mountains is highlighted by the yellow band. Dab. – Dabis Formation; Nom. – Nomtsas Formation. Zaris Sub-basin members: 1. Kanies, 2. Omkyk, 3. Hoogland, 4. Urikos, 5. Niederhagen, 6. Vingerbreek, 7. Kreyrivier, 8. Niep; Witputs Sub-basin members: 1. Kanies, 2. Mara, 3. Kliphoek-Aar, 4. Mooifontein, ?. possible depositional hiatus, 5. Niederhagen, 6. Vingerbreek, 7. Nasep, 8. Huns, 9. Feldschuhhorn, 10. Spitskop. Named $\delta^{13}C_{carb}$ excursions: BANE – Basal Nama negative excursion; OME – Omkyk positive excursion; SPIE – Spitskop positive excursion. OS1, OS2, K1, K2: major sequences after (Saylor et al., 1995; Adams et al., 2005). See Fig. 3 for key to lithostratigraphy. (C) Revised geological map of the Tsaus Mountains based on lithostratigraphic correlation, field observations of structural tectonics and observed fault extent using satellite and aerial photography. Map shows positions of key sections sampled for chemostratigraphy. See Figs S2-S3 for expanded Nama Group section correlation and high resolution, revised geological maps, superimposed upon satellite images (GoogleEarth 2023, Maxar Technologies).

1983; Saylor et al., 1995). The Nama Group succession of the Neint Nababeep Plateau outcrops across the Orange River border in southern Namibia and northwestern South Africa (Fig. 2A; Germs, 1983; Nelson et al., 2022). Here, strata may record deposition in a contiguous ('Vioolsdrif') sub-basin that was partially separated from the Witputs Sub-basin by a second paleobathymetric high (the 'Koedoelaagte Arch'), or represent deposition within the southernmost extent of the Witputs Sub-basin (Germs and Gresse, 1991; Germs et al., 2009; Nelson et al., 2022).

2.1. Stratigraphy of the Kuibis Subgroup, and published occurrence of Cloudina

The Kuibis Subgroup is subdivided into the Dabis and overlying Zaris formations (Germs, 1983; Saylor et al., 1995). In the Zaris Sub-basin, generally thin (<25 m) coarse clastic deposits of the Dabis Formation (Kanies Member) and the carbonate-dominated Zaris Formation (Omkyk and Hoogland members) record diachronous deposition across the Proterozoic granitic basement and development of a storm- and wave-dominated carbonate ramp during ongoing marine transgression (Saylor et al., 1998; Smith, 1999; Grotzinger, 2000; Dibenedetto and Grotzinger, 2005; Wood et al., 2015). In the Witputs Sub-basin, the Dabis Formation (Kanies, Mara, Kliphoek and Aar members) and Zaris Formation (Mooifontein Member) preserve two major sequences (K1 and K2), with coarse siliciclastic-dominated lowstand deposits overlying sequence boundaries (Kanies and lower Kliphoek members) and fine siliciclastic and carbonate-dominated transgressive to highstand deposits (Mara, Aar and Mooifontein members; Figs. 2B, S3; Saylor et al., 1995; Hall et al., 2013). Sequence boundaries are commonly overlain by coarse siliciclastic lowstand deposits in more proximal, eastern exposures, but correlative conformities complicate the lateral association of member boundaries in deeper, more continuous sections to the west (Saylor et al., 1995).

Litho- and chemostratigraphic correlation of Kuibis Subgroup strata between the Zaris and Witputs sub-basins supports contemporaneous deposition of the Omkyk Member with the Kliphoek, Aar and Mooifontein members (K2; Saylor et al., 1998; Wood et al., 2015). The only dated ash bed from the Kuibis Subgroup derives from the lower Hoogland Member of the Zaris Formation in the Zaris Sub-basin and yields a zircon U-Pb age of 547.36 ± 0.31 Ma (Bowring et al., 2007). Given that no ash bed has yet been confirmed from the Kuibis Subgroup of the Witputs Sub-basin, this interbasinal correlation constrains a likely minimum age of 547.36 ± 0.31 Ma for deposition of the uppermost Mooifontein Member (Saylor et al., 1998; Bowring et al., 2007).

The stratigraphically lowest occurrence of *Cloudina* has previously been documented from the Mara Member of the Witputs Sub-basin (Germs, 1983), but the precise location of this occurrence and its position relative to the regional $\delta^{13}C_{carb}$ profile, remain undocumented. At present, sections with associated chemostratigraphic data record the lowest occurrence of *Cloudina* in limestones of the lower Omkyk Member (OS1) of the Zaris Sub-basin that immediately postdate recovery (>0‰) from the BANE (Figs. 2B, S3; Saylor et al., 1998; Smith, 1999; Wood et al., 2015; Bowyer et al., 2022).

2.2. Regional geological setting of the Tsaus Mountains

The Tsaus Mountains cover an area of ca. 11 km^2 and outcrop within the Tsau Khaeb National Park, 10 km to the west/northwest of Farm Grens, and 50 km to the southwest of the fossiliferous section on Farm Aar (Figs. 2A, C, S3). The succession exposed in the Tsaus Mountains therefore represents the most westerly outcrop of the Witputs Sub-basin investigated to date. The lower Kuibis Subgroup was deposited diachronously from west to east during initial transgression onto the Proterozoic basement (Germs, 1983; Saylor et al., 1995). As such, the Tsaus Mountains succession should preserve some of the oldest Nama Group strata corresponding to the lower K1 sequence and, depending on their absolute age, basal clastic deposits may have the potential to host soft-bodied fossils of the preceding White Sea assemblage biozone (Figs. 1, S1).

3. Methods

3.1. Stratigraphic logging and geochemical sampling

Sampling was undertaken at three well exposed sections (MTa-c) that outcrop in the eastern limb of the Tsaus Mountains (Figs. 2C, 3, S4A). Sedimentary logging and geochemical sampling were carried out systematically from the base to the top of each section, with sampling heights determined through use of a folding meter stick. Thumb sized geochemical samples (~25–35 g) were collected at 0.5–1 m resolution, where possible. Distinctive and laterally continuous marker horizons were identified at six stratigraphic levels between MTa and MTc, and within the central limb of the Tsaus Mountains (Fig. 3). Throughout the geochemical sampling campaign, exposed bedding planes and float samples were systematically and non-destructively examined, and additional paleontological information was recorded. Fossil specimens were photographed in the field but not removed from the outcrop, with the exception of some float specimens, which are catalogued and repositioned at the Geological Survey of Namibia (Windhoek) or the University of Namibia (Keetmanshoop).

3.2. Identification of Member boundaries, sequence boundaries, stratal stacking patterns

The Kuibis Subgroup in the Witputs Sub-basin has been subdivided into formations and members based on an integrated lithostratigraphic and sequence stratigraphic architecture (Germs, 1974, 1983; Saylor et al., 1995). The K1 sequence comprises siliciclastic-dominated lowstand deposits of the Kanies Member and carbonate-dominated transgressive deposits of the Mara Member (Saylor et al., 1995). The Kanies and Mara Members are therefore separated by a transgressive surface that marks the first major flooding surface following the lowstand systems tract. The K1 and overlying K2 sequences are separated by a sequence boundary, which also defines the boundary between the carbonate-dominated Mara Member and overlying siliciclastic lowstand deposits of the Kliphoek Member (Saylor et al., 1995). Whilst planar stratified to large-scale cross-stratified sandstones characterise lowstand deposits of the Kliphoek Member to the east, these transition down-dip to interbedded sandstones and carbonates to the west, wherein the distinction between lowstand and early transgressive deposition is less clear (Saylor et al., 1995; Wood et al., 2015). Within the K2 sequence, a second transgressive surface separates coarse lowstand deposits of the Kliphoek Member in shallow sections from transgressive deposits of the mixed carbonate-siliciclastic Aar Member, which themselves transition to the carbonate-dominated Mooifontein Member (Saylor et al., 1995; Hall et al., 2013).

Here, we extend this correlation framework further to the west, into the Tsau Khaeb National Park. Firstly, small-scale shallowing-up cycles (parasequences) bounded by flooding surfaces were identified and measured in the field during stratigraphic logging at MTa-c. These consist of thin-bedded and commonly recessive intervals composed of finer-grained sediments that transition to medium-thick bedded intervals of more resistant, coarser-grained sediments. Depositional sequences K1 and K2 of Saylor et al. (1995) were identified in the Tsaus Mountains through assessment of vertical facies changes that inform large-scale stratal stacking patterns. Finally, we interrogated the stratal stacking patterns of published stratigraphic logs to the east of the Tsaus Mountains to develop a lateral correlation framework and Member subdivision that is consistent with the sequence stratigraphic framework of Saylor et al. (1995).

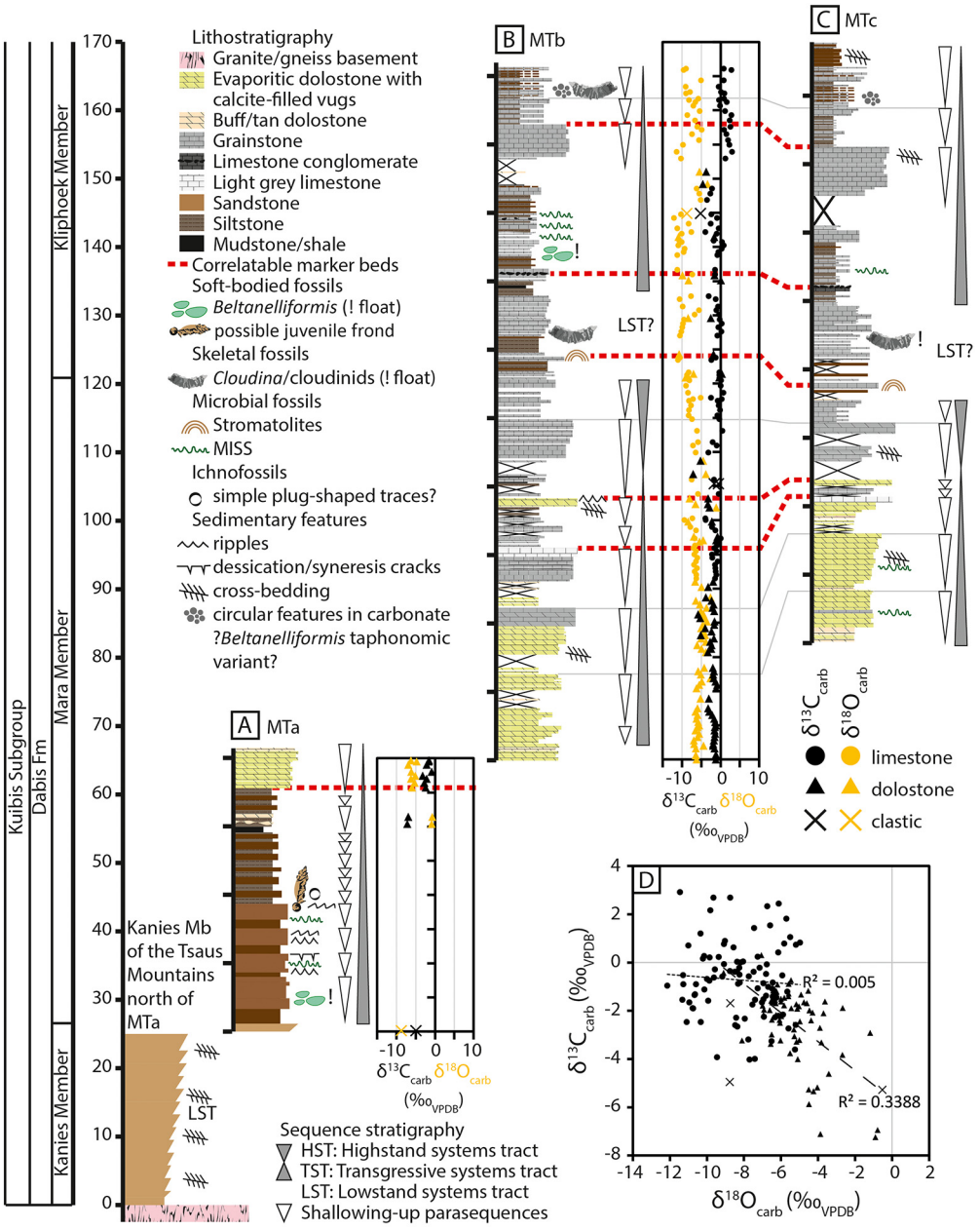

Fig. 3. Individual measured sections from the eastern limb of the Tsaus Mountains (see section locations in Fig. 2C), relative to composite height (at left). (A)-(C) Lithostratigraphy, paleontology and $\delta^{13}C_{carb}$ and $\delta^{18}O_{carb}$ chemostratigraphy of (A) MTa, and (B) MTb sections. (C) Lithostratigraphy and paleontology of MTc section. Dashed red lines that connect (A)-(C) show lateral correlation of continuous marker horizons, discussed in the text. (D) Cross-plot of $\delta^{13}C_{carb}$ and $\delta^{18}O_{carb}$ for all samples. R^2 values in (D) correspond to limestones (circles, dotted line) and dolostones (triangles, dashed line).

3.3. Carbonate $\delta^{13}C$ chemostratigraphy

Carbonate samples collected from MTa and MTb sections were analyzed for their carbonate carbon and oxygen isotope ratios. Carbonate powders were microdrilled from fresh surfaces, targeting the finest microcrystalline material. Veins, fractures, and calcite cement infilling vugs in dolostone were avoided. The resulting powders were analyzed by continuous flow elemental analyzer isotope ratio mass spectrometry (CF-EA-IRMS) at the University of Edinburgh Wolfson Laboratory, or at Iso-Analytical Ltd. Carbon and oxygen isotope ratios were also analyzed from carbonate cements within five clastic samples, two of which are discounted (see Supplementary Information). Calcium carbonate concentrations (% $CaCO_3$ equivalent) for clastic samples were calculated based on beam intensities after CO_2 production relative to the mean of CO_2 peak area of powdered standards of known $CaCO_3$ concentration, normalized to the mass of sample analyzed. Replicate measurements of standards (n = 39) yielded an uncertainty of ±2.6%. Data from clastic samples are differentiated from limestone and dolostone samples in all figures and Table S2. All data are reported in per mil notation relative to the composition of Vienna Pee Dee Belemnite (VPDB) (Table S2). Replicate analyses of samples and standards yielded standard deviations (1σ) of better than ±0.08‰ for $\delta^{13}C$ and better than ±0.12‰ for $\delta^{18}O$.

4. Results

4.1. Lithological succession of the Tsaus Mountains

The Tsaus Mountains succession consists of the Kanies, Mara and Kliphoek members of the Dabis Formation. Although the Mooifontein Member is shown on the currently published geolog-

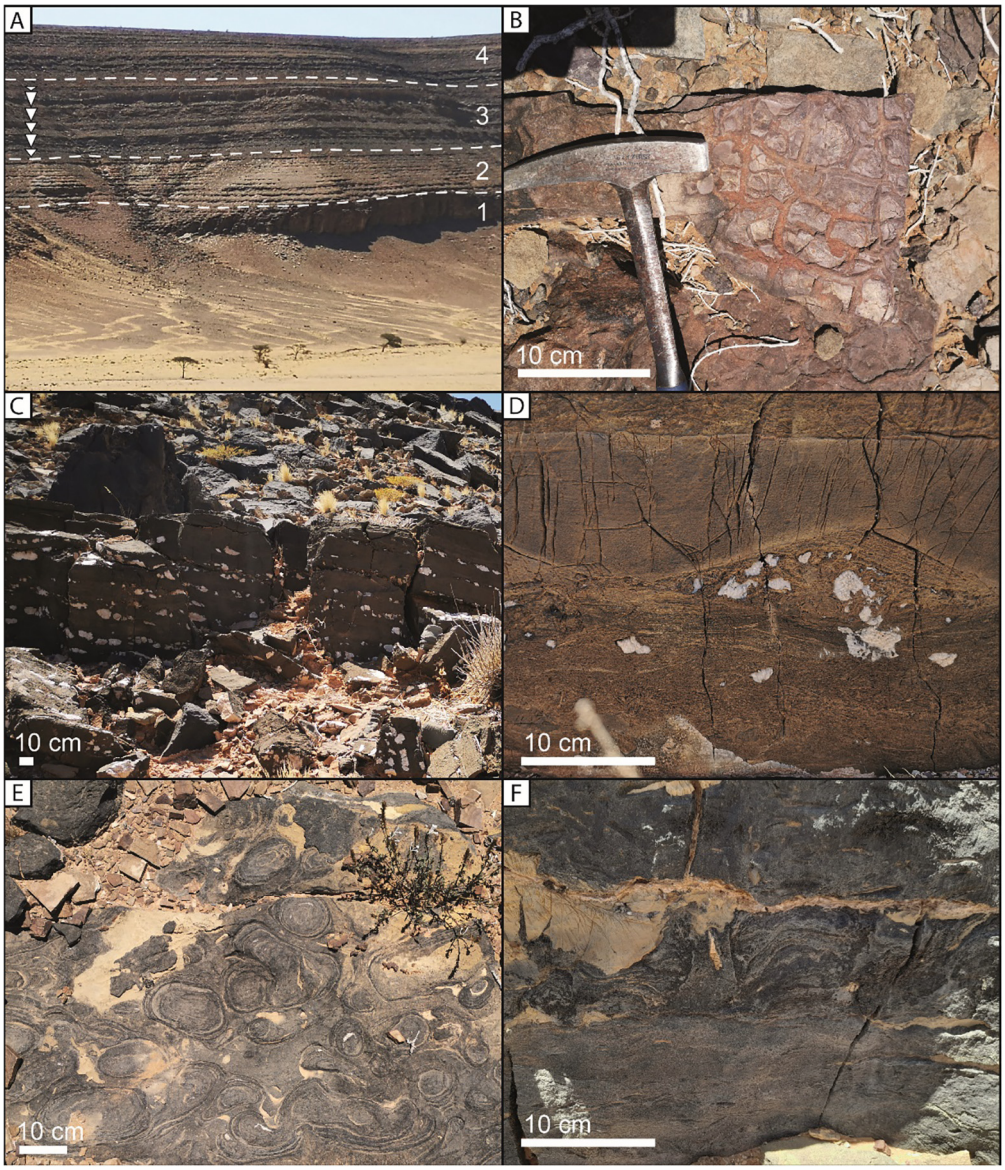

Fig. 4. (A) Outcrop photograph showing stratigraphic subdivision, with (1) Kanies Member, (2) siliciclastics of the lower Mara Member, (3) carbonates of the middle to upper Mara Member, (4) mixed siliciclastics and carbonates of the Kliphoek Member. Triangles to the left of (3) highlight shallowing-up parasequences visible within the middle to upper Mara Member. (B) Mudcracks in sandstone of the basal Mara Member Member (MTa section). (C) Abundant calcite-filled vugs pepper the upper vuggy dolostone marker bed, Mara Member (MTb section). (D) Rip-up clasts, megaripples and abundant calcite-filled vugs within the upper part of the upper vuggy dolostone marker bed, Mara Member (MTb section). (E) Stromatolitic limestone marker bed (MTb section). (F) Cross section of stromatolitic limestone marker bed showing eroded upper surface and abundant rip-up clasts in overlying limestone bed (MTb section).

ical map of the Tsaus Mountains, it is in fact not present (Figs. 2C, S2, S3).

Kanies Member

In northern exposures of the central and eastern limbs of the Tsaus Mountains, the basal Kanies Member consists of yellow-weathering, pebbly to very coarse, planar to cross-bedded sandstones, followed by ca. 27 m of coarse- to medium grained, planar-bedded sandstone, where stacks of resistant beds (0.5–1.5 m thick) commonly form cliffs (Figs. 3, 4A). Conglomeratic sandstones that characterize basal Kanies Member deposits in more proximal sections to the east (Saylor et al., 1995) are absent.

Mara Member

A transgressive surface defines the base of the Mara Member (Saylor et al., 1995), which is overlain by planar-bedded fine- to medium-grained sandstone arranged in four coarsening-up cycles, with symmetrical ripples, occasional asymmetrical and interference ripples, and some bedding plane surfaces with polygonal mud cracks (Fig. 4B). Nine cycles of recessive, thin- to medium-bedded grey fine grained sandstone and siltstone follow, with two buff-weathering dolostone interbeds, the first of which is lenticular and laterally discontinuous (Fig. 3A). This is followed by an interval of mid-grey, often cross-bedded, non-ferroan dolostone with subordinate interbeds of buff-weathering, ferroan dolostone, dominated by small-scale shallowing-upward cycles. Dolostone beds commonly exhibit pressure solution features, and vugs infilled by calcite or (less commonly) silica cement are abundant on bedding plane surfaces and in exposed sections perpendicular to bedding (Fig. S4B). These cement-filled vugs are commonly 2–3 cm in diameter, but rare silica-cemented lenticular/nodular structures may be up to 35 cm wide. Calcite-filled vugs commonly cross-cut sedimentary features, suggestive of matrix replacement, but in some instances, darker laminations in the dolostone matrix also drape over vuggy calcite infill, suggesting penecontemporaneous

formation prior to lithification (Fig. S4B). An interval of mid-light grey, thin- to medium-bedded limestone follows, with subordinate limey dolostone, brown-weathering dolostone, and calcite-filled vugs (Fig. 3B). The approximate level of this transition is distinguished by a prominent pale grey mottled limestone bed at ca. 95 m, which serves as a useful laterally-continuous and traceable marker bed (Figs. 3B, C). At ca. 102 m, a striking ca. 1 m-thick brown-weathering mid-grey dolostone bed serves as another readily correlatable marker horizon that can be traced across the entire Tsaus Mountains outcrop (herein termed the 'upper vuggy dolostone marker bed'; Figs. 3B, C, 4C). This marker bed contains calcite-filled vugs that are commonly ≥10 cm in diameter (Fig. 4C), and an upper unit containing abundant rip-up clasts and megaripples with exceptionally preserved foreset laminae (Fig. 4D). Overlying this marker bed are two parasequences consisting of thin-bedded mid-grey limestone with subordinate light brown weathering dolostone and limey dolostone (Fig. 3B, C).

Kliphoek Member

A ca. 1.5 m-thick interval of siltstone and fine sandstone marks the base of the Kliphoek Member, followed by a distinctive mid-grey limestone bed with circular to lenticular/irregular stromatolitic cross sections (Fig. 3B, C). These stromatolites range from <10 cm to >40 cm in diameter and occasionally show evidence for reworking and partial dolomitization (Fig. 4E, S4C, D). This stromatolitic limestone bed serves as a third marker horizon that is laterally traceable throughout the entire Tsaus Mountains outcrop (Figs. 3B, C, S4E). Exposed bedding planes and bed cross-sections clearly show erosion of stromatolite heads prior to deposition of an overlying thin limestone bed with matrix-supported flat pebbles (Fig. 4F). This is overlain by interbedded thin- to medium-bedded mid-grey limestone with common microbial textures and occasional wavy bedding, siltstone, fine sandstone, and rare mudstone/shale. Within this interval, a 15 cm-thick, matrix-supported limestone conglomerate with rounded to sub-rounded limestone and dolomudstone clasts (Fig. S4F), is also laterally correlatable between MTb and MTc sections (Fig. 3B, C). A final marker horizon is present at ca. 154 m, and comprises a 4–6.5 m-thick resistant interval of medium-bedded limestone with occasional cross-cutting fractures filled with calcite cement (Fig. 3B, C). This is followed by a recessive interval of thinly interbedded limestone, siltstone and sandstone (Fig. 3B, C), with an additional recessive and flaggy cross-bedded quartzite capping the succession at MTc (Fig. 3C).

4.2. Distribution of biota

The lower Mara interval at MTa and neighboring sections within the Tsaus Mountains contains numerous bedding planes with textures that likely reflect microbially-induced sedimentary structures, possible plug-shaped ichnofossils, and forms that may represent soft-bodied metazoans (Fig. 3A; Wood et al., 2023). The latter include examples of *Beltanelliformis* and a possible juvenile uniterminal rangeomorph or arboreomorph frond and associated holdfast (Wood et al., 2023).

No fossils were identified within the lower ca. 60 m at MTb or ca. 40 m at MTc, corresponding to the Mara Member interval dominated by vuggy dolostone and overlying limestone that underlies the stromatolitic limestone marker bed in each section (Fig. 3B, C). The lowest occurrence of *Cloudina* is found in the lowermost Kliphoek Member, at ca. 63.3 m in the MTb section (composite height ca. 128.3 m; Figs. 3B, 5A). Float samples with abundant *Cloudina* are also found in this interval at MTc, bracketed below and above by the stromatolitic marker bed and limestone conglomerate, respectively (Figs. 3C, 5B). Above the limestone conglomerate at MTb, the bedding plane of a thin carbonate float sample is populated by closely spaced and sharply defined circular features with flat upper surfaces, preserved in positive epirelief (Figs. 3B, 5C). These features were also found preserved in float sandstone at the same stratigraphic level in the north-central limb of the Tsaus Mountains (Fig. 5D), and both specimens may represent taphonomic variants of *Beltanelliformis*.

Cloudina are also found within the final flaggy, thin-bedded plateau interval of the Kliphoek Member at MTb, above the thick limestone marker bed (Fig. 3B). Also within this interval at MTb is an in-situ limestone bed that contains clustered circular structures (<1 cm in diameter) that have a narrow size distribution and are commonly infilled by white calcite cement (Fig. 5E). The biological affinity of these structures remains uncertain. However, approximately the same stratigraphic position at MTc hosts thin limestone beds that contain similar sized circular structures (Figs. 3C, 5F), of which the flat upper surfaces, sharply defined edges and overall distribution are reminiscent of *Beltanelliformis*.

4.3. Carbon isotope chemostratigraphy of the Tsaus Mountains

Fig. 3 presents new $\delta^{13}C_{carb}$ and $\delta^{18}O_{carb}$ data from dolostone and limestone samples, in addition to data from carbonate cements from three siliciclastic samples at MTa and MTb sections (Table S2). Carbonate samples yield $\delta^{13}C_{carb}$ from −7.24‰ to +2.91‰ and $\delta^{18}O_{carb}$ from −12.14‰ to −0.78‰. Scattered values of $\delta^{13}C_{carb}$ are superimposed upon a general increase up-section, with a prominent shift at ca. 152 m from dominantly negative to dominantly positive $\delta^{13}C_{carb}$.

The stratigraphically lowest data point ($\delta^{13}C_{carb}$ = −4.95‰) derives from carbonate cement within a coarse sandstone bed ($CaCO_3$ = 15.07 wt%) of the upper Kanies Member at the base of MTa (ca. 25.3 m; Figs. 3A, 6). Two buff coloured dolostone interbeds near the top of the overlying siliciclastic-dominated interval (ca. 55–57 m) yield significantly depleted $\delta^{13}C_{carb}$ (minimum = −7.24‰) and notably enriched $\delta^{18}O_{carb}$ (maximum = −0.74‰). Overlying dolostones, limey dolostones and limestones, up to the level of the upper vuggy dolostone marker bed (ca. 61–102 m), yield negative $\delta^{13}C_{carb}$ ($\delta^{13}C_{carb}$ = −5.88‰ to −0.09‰, mean = −2.13‰; $\delta^{18}O_{carb}$ = −9.45‰ to −1.19‰, mean = −5.77‰). Data in this interval may show cyclicity, whereby the lowest $\delta^{13}C_{carb}$ values are commonly recorded within intervals dominated by thinly bedded carbonate immediately above minor flooding surfaces (e.g., 72–74 m, 80.72 m, and 88.50–90.50 m; Fig. 3B). However, this pattern is obscured by scattered negative values in a sulfurous, vuggy dolostone and limey dolostone interval nearing the top of a parasequence (83.22–86.22 m), and is not apparent in the thin bedded interval immediately overlying the light grey limestone marker bed (95.5–97.5 m), where values are notably enriched (−1.66‰ to −0.09‰; Fig. 3B). Samples of the upper vuggy dolostone marker bed yield $\delta^{13}C_{carb}$ from −3.38‰ to −3.24‰ and $\delta^{18}O_{carb}$ from −8.11‰ to −6.57‰.

Two limestone samples ($\delta^{13}C_{carb}$ = −0.54‰ and −1.74‰; $\delta^{18}O_{carb}$ = −5.93‰ and −7.54‰) that immediately overlie the upper vuggy dolostone marker bed bracket a carbonate cemented clastic sample ($CaCO_3$ = 68.59 wt%) recording similar $\delta^{13}C_{carb}$ (−1.69‰) despite anomalously elevated $\delta^{18}O_{carb}$ (−0.52‰). Values of $\delta^{13}C_{carb}$ increase throughout the overlying ca. 6.30 m (106–114 m), from −7.12‰ in a thin dolostone bed within a recessive interval, to +0.41‰ in medium-bedded limestone. The following ca. 8.60 m-thick interval of thin-bedded limestone and subordinate dolostone that underlies the stromatolitic limestone marker bed, is characterised by $\delta^{13}C_{carb}$ values that oscillate about a mean of −0.40‰ ($\delta^{13}C_{carb}$ = −2.59‰ to +0.62‰). Overlying samples from the *Cloudina*-bearing interval bracketed by the stromatolitic limestone and limestone conglomerate marker beds yield lower mean $\delta^{13}C_{carb}$ (−1.19‰) in the range −3.20‰ to +0.20‰. This trend of oscillatory, but gradually decreasing $\delta^{13}C_{carb}$ culminates in a more prominent downturn within the interval domi-

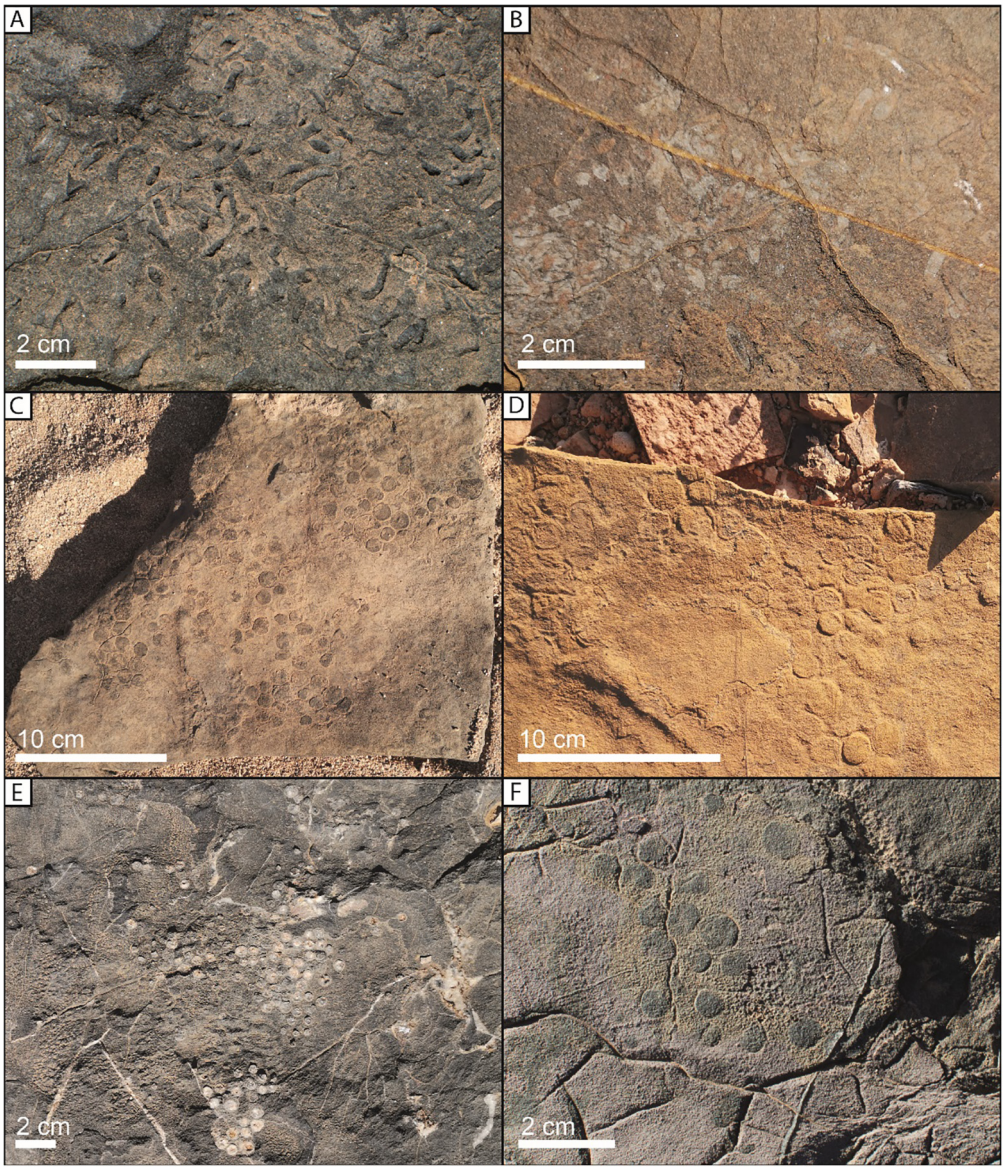

Fig. 5. Biota of the Kliphoek Member at MTb and MTc sections. (A) *Cloudina* exhibiting characteristic cone-in-cone morphology (in-situ bed, MTb section height 63.3 m). (B) Float sample with *Cloudina* (MTc section height 43.15 m). (C) Thin carbonate float sample containing circular impressions of probable *Beltanelliformis* (/*Nemiana*) (MTb section height 74 m). (D) Sandstone float sample with circular features (probable *Beltanelliformis*) in central-north limb of Tsaus Mountains (immediately south of marker 'Tsaus 1227', Fig. 2C), within interval above limestone conglomerate and below thick limestone marker bed. (E) In-situ limestone bed containing clustered circular structures (MTb section height 97.72 m). (F) Limestone float sample containing clustered circular structures (MTc section height 79.55 m).

nated by thinly interbedded limestones, siltstones and sandstones, to reach a nadir of −4.61‰ at ca. 150 m, immediately below the thick limestone marker bed (Fig. 3B). A carbonate cemented clastic sample ($CaCO_3 = 29.35$ wt%) at ca. 145 m yields values of $\delta^{13}C_{carb}$ (−5.28‰) and $\delta^{18}O_{carb}$ (−8.75‰) that approximate data from bracketing limestone samples (Fig. 3B). Carbonate samples within the upper part of this negative $\delta^{13}C_{carb}$ excursion (ca. 147–151 m) are characterised by notably elevated $\delta^{18}O_{carb}$ (−6.31‰ to −3.42‰, mean = −5.21‰) relative to underlying and overlying samples (Fig. 3B).

A shift from dominantly negative to dominantly positive $\delta^{13}C_{carb}$ is recorded near the base of the thick limestone marker bed, or within the top of the underlying recessive, covered interval (ca. 152 m). This shift at ca. 152 m also marks a return to more negative $\delta^{18}O_{carb}$ (Fig. 3B). Values of $\delta^{13}C_{carb}$ remain dominantly positive throughout the remaining ca. 13 m (−0.59‰ to +2.91‰, mean = +1.25‰), with minimum values recorded at the approximate position of the in-situ limestone bed containing clustered circular structures (Figs. 3B, 5E).

Stratigraphic trends in isotopic data show consistency within and between lithologies (Fig. 3A, B). Whilst a general negative correlation between $\delta^{13}C_{carb}$ and $\delta^{18}O_{carb}$ is resolved stratigraphically (Fig. 3A, B), neither limestone nor dolostone samples independently show significant correlation between $\delta^{13}C_{carb}$ and $\delta^{18}O_{carb}$ (Fig. 3D), nor is any correlation significant when limestone and dolostone samples are considered together ($R^2 = 0.2446$).

5. Discussion

5.1. Stratigraphic correlation and facies evolution of the Kuibis Subgroup, Witputs Sub-basin

The transgressive surface that marks the base of the Mara Member is commonly associated with the first appearance of carbonates, or interbedded siltstones and carbonates, in sections to

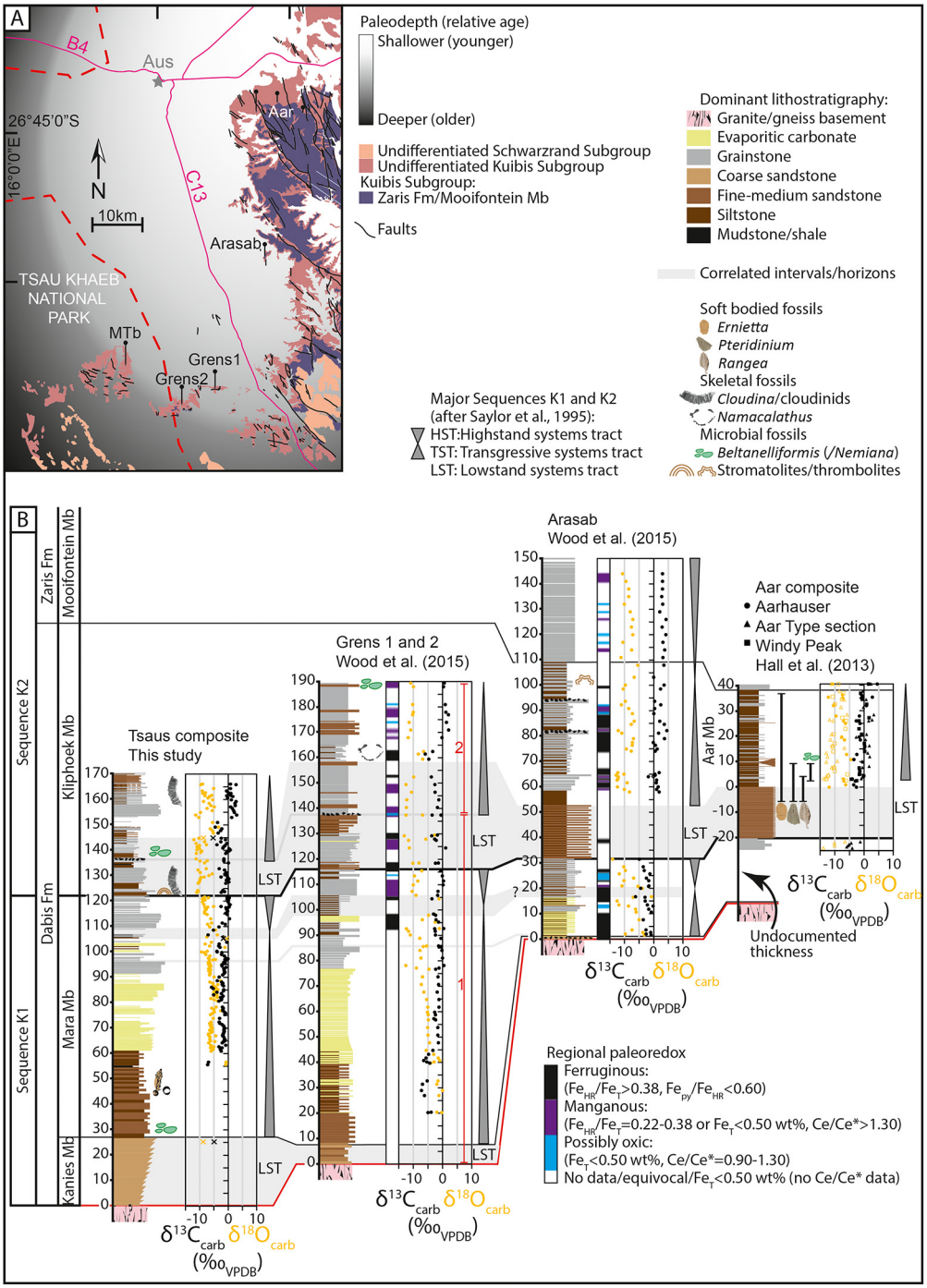

Fig. 6. Lithostratigraphic and chemostratigraphic correlation, documented fossil occurrences and summarized paleoredox interpretations for sections deposited on the western edge of the Witputs Sub-basin. Inset map shows positions of sections and relative paleodepth. Regional paleoredox interpretation for sections on farms Grens and Arasab after interpretation of combined Fe-speciation and Ce/Ce* data (Wood et al., 2015; Tostevin et al., 2016). See text for discussion concerning Member boundary designations and Figs S2-S3 for expanded section correlation.

the east and south of Tsaus. At Tsaus, this major transgressive surface is defined in outcrop (ca. 27 m) at the base of a fining-up, siliciclastic-dominated package (Figs. 3A, 6). Transgression coincident with deposition of the lower Mara Member pushed the siliciclastic shoreline landward (Saylor et al., 1995), and shifted the environment of deposition at Tsaus from proximal shoreface to shallow marine. Similarly, at closely neighbouring sections to the east of Tsaus, the transgressive surface (and corresponding Kanies/Mara boundary) may be more accurately placed where the average grain size of siliciclastic packages begins to decrease (Figs. 6A, B). This is a reassessment of the current interpretation based on the defining characteristics of Dabis Formation subdivision (Saylor et al., 1995; Wood et al., 2015). The lower Mara Member at Tsaus and Grens was deposited during diachronous transgression, and this interval is associated with subaerial exposure and non-deposition or non-preservation due to erosion at more proximal, easterly sections (Figs. 6A, B, 7A).

Thin- to medium-bedded dolostones that immediately overlie clastics of the lower Mara Member at Tsaus commonly contain vugs infilled by calcite cement (Fig. 4C, S4B). Observed relationships between the vugs and host dolostone suggest that they formed penecontemporaneously, prior to lithification, and they

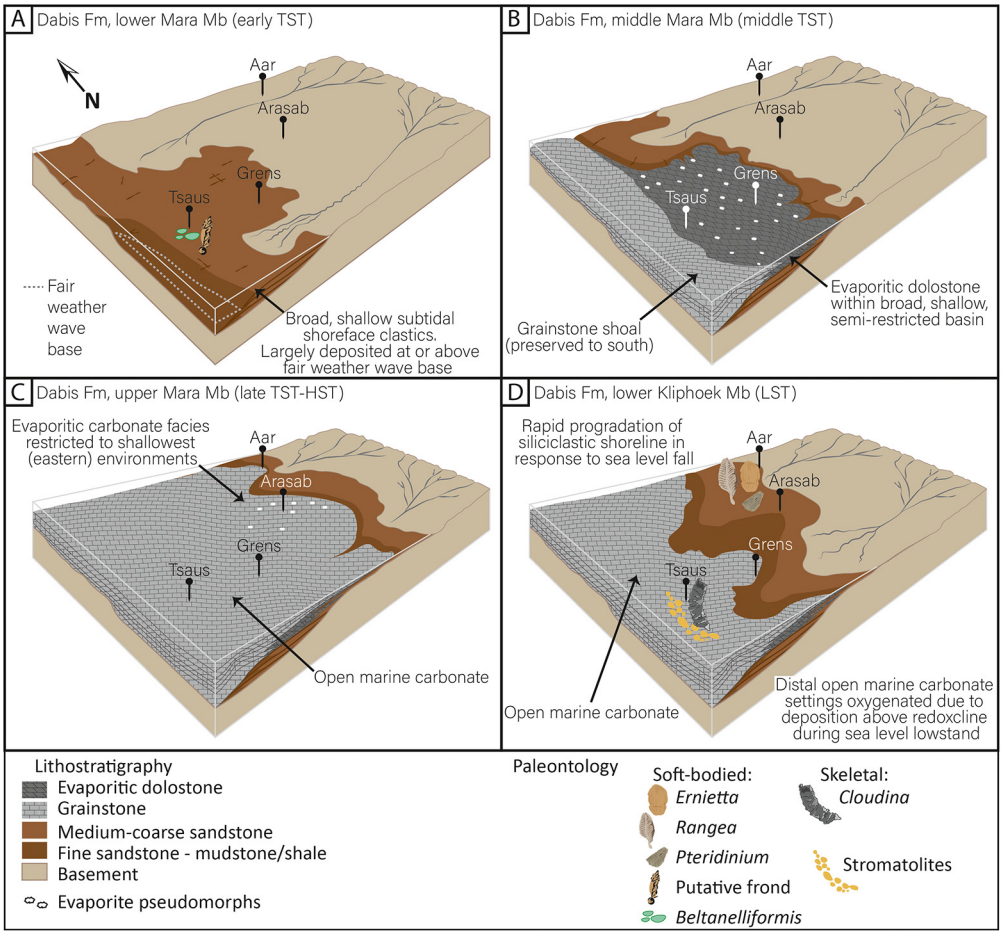

Fig. 7. Interpreted facies evolution of the Kuibis Subgroup of the Witputs Sub-basin between Farm Aar (proximal) and the Tsaus Mountains (distal), and inferred sequence stratigraphy. (A) Following the deposition of coarse clastics of the Kanies lowstand, the initiation of marine transgression led to the diachronous deposition of rippled sandstones and siltstones within a broad, shallow shoreface environment at Tsaus and Grens. These deposits are here assigned to the lower Mara Member, and fine upwards with increasing distance from the shoreline. (B) Continued marine transgression led to the deposition of dolostone of the middle Mara Member within a broad, shallow, evaporitic basin that was prone to partial restriction from the open ocean, possibly related to the development of an offshore barrier bar/shoal. (C) Maximum flooding within the upper Mara Member led to the transition from evaporitic dolostone to open marine limestone at Tsaus and Grens, and the diachronous deposition of shallow evaporitic and subsequent open marine carbonate facies at more proximal sections on farms Arasab and Aar. (D) Sea level fall led to rapid progradation of the siliciclastic shoreline, deposition of thick lowstand clastics of the Kliphoek quartzite at farms Aar and Arasab, and mixed distal shoreface clastics and open marine carbonates at Tsaus and Grens. Shallow, proximal depositional environments hosted soft-bodied fossils of *Rangea*, *Pteridinium*, *Ausia* and *Ernietta*, and the skeletal *Cloudina* grew contemporaneously in lateral carbonate environments, with inferred widespread oxygenation of all settings.

are herein interpreted to represent pseudomorphs after evaporite (e.g., gypsum). Evaporitic fabrics have been previously noted from the Mara Member at Grens (Fig. 6B). The abundance of evaporite pseudomorphs and absence of karst surfaces at Tsaus and at Grens strongly support deposition of the Mara Member dolostone within a shallow intertidal, and occasionally semi-restricted hypersaline environment, with occasional evidence for storm reworking, consistent with the interpretation of some transgressive K1 deposits after Saylor et al. (1995). This is particularly important for the interpretation of carbonate-based isotope proxies in the Mara Member dolostone as indicators of global ocean chemistry (see section 5.3). No evaporite pseudomorphs have been noted from the lower Mara Member in sections to the south of Tsaus (e.g., Witputs, Fig. S3; Saylor et al., 1995). Indeed, there, calcarenite and trough cross-stratified ooid grainstone may instead record the presence of an open marine barrier shoal (Figs. 7B, S3; Saylor et al., 1995).

Ongoing transgression led to the gradual appearance of limey dolostone and limestone beds at Tsaus and Grens, and shifted the locus of major evaporite precipitation to recently flooded, shallower environments to the east (e.g., Arasab, Figs. 6A, B, 7C). The maximum flooding surface of sequence K1 is likely within the recessive and poorly exposed interval of the Mara Member, above the upper vuggy dolostone marker bed at Tsaus, and within correlative intervals of thinly interbedded mudstone and dolostone at Grens and Arasab (Fig. 6B).

The base of the Kliphoek Member, marked by the K2 sequence boundary, is commonly overlain by large-scale cross-stratified, conglomeratic or pebbly sandstones (in proximal, eastern exposures), or interbedded trough cross-stratified, coarse sandstone, thinly-bedded calcisiltite, calcarenite, and/or trough cross-stratified ooid grainstone (in distal, western exposures; Saylor et al., 1995). This sequence boundary represents a fall in relative sea level that resulted in rapid progradation of the siliciclastic shoreline and deposition of coarse clastics atop carbonate of the Mara Member (Fig. 7D; Saylor et al., 1995). In distal sections (e.g., Swartkloofberg; Fig. S3), where the lower Kliphoek Member consists of interbedded sandstone and calcarenite, the K2 sequence boundary (Mara/Kliphoek boundary) is placed at the base of the lowest bed of coarse sandstone (Germs and Gresse, 1991; Saylor et al., 1995). At Tsaus, this level corresponds to a sandstone bed (ca. 122 m) immediately underlying the stromatolitic limestone marker bed (Figs. 3B, 6B). Similarly, at Grens, an equivalent reassessment of Member subdivision places the Mara/Kliphoek boundary at the

base of a 2 m-thick unit of interbedded platy quartzite and siltstone (Fig. 6B). Whilst no stromatolitic marker horizon has been observed above this level at Grens, the overall lithostratigraphic sequence and sedimentology are similar to the Tsaus succession, including a limestone breccia that may correlate with the limestone conglomerate bed at Tsaus (Figs. 6B, S4F). The lithostratigraphy and sedimentology throughout this interval at both Tsaus and Grens are indicative of shallow marine deposition, with evaporitic and tepee structures at Grens, erosion and reworking of stromatolite heads at Tsaus, and occasional sheets of sandstone and siltstone at both sites that likely reflect the influx of proximal flood-derived clastics.

5.2. Environmental controls on biotic distribution

Regionally, we infer that continued marine transgression led to the deposition of dolostone of the middle Mara Member within a broad, shallow, evaporitic basin that was prone to partial restriction from the open ocean, possibly related to the development of an offshore barrier bar/shoal (Figs. S2, S3). Maximum flooding within the upper Mara Member led to the transition from evaporitic dolostone to open marine limestone at Tsaus and Grens, and the diachronous deposition of shallow evaporitic and subsequent open marine carbonate facies at more proximal sections on farms Arasab and Aar.

Sea level fall during the subsequent lowstand of basal sequence K2 led to rapid progradation of the siliciclastic shoreline and deposition of the thick Kliphoek quartzite in shallow settings (Fig. 6B). In sections that preserve these proximal deposits (e.g., Farm Aar), the Kliphoek quartzite contains soft-bodied fossils including, but not limited to, *Ernietta*, *Pteridinium*, *Rangea*, and *Ausia* (Gürich, 1930; Pflug, 1966; Hahn and Pflug, 1985; Hall et al., 2013; Vickers-Rich et al., 2013). A laterally and temporally correlative interval at Tsaus hosts the lowest recorded occurrence of *Cloudina* in more distal (deeper) carbonates (limestones) (see below; Figs. 5A, B, 6B, 7D). This is in broad agreement with the original lithostratigraphic correlation of Germs (1974, 1983), who recognised that soft-bodied fossils and skeletal *Cloudina* of the basal Nama succession coexisted in laterally-correlative clastic and carbonate depositional environments, respectively.

In proximal sections near farms Aar and Arasab (Fig. 6A, B), coarse lowstand siliciclastics of the Kliphoek quartzite transition to thinly interbedded sandstones, mudstones and limestones of the Aar Member, which together record the K2 transgression (Saylor et al., 1995; Hall et al., 2013). At Farm Aar and neighbouring sections, sandstone beds throughout the Aar Member commonly contain soft-bodied fossils, including *Pteridinium*, *Ernietta*, *Rangea*, and *Beltanelliformis* (Hall et al., 2013; Vickers-Rich et al., 2013). Within the same interval, carbonates contain *Cloudina* at Tsaus and *Namacalathus* at Grens, and specimens of *Beltanelliformis* are reported from sandstone layers at Grens, but may also be present on carbonate bedding planes at Tsaus (Figs. 5F, 6B). The preservation of *Beltanelliformis* in both siliciclastic and carbonate beds in the Nama Group is documented here for the first time (Figs. 5C, D). Large, three dimensionally preserved soft-bodied biota from this interval (e.g., *Ernietta*, *Rangea*) are most commonly preserved as transported individuals within flood-derived sheet sandstones or gutter casts, whereas *Beltanelliformis* has only been reported in-situ from bedding surfaces (e.g., Hall et al., 2013; Wood et al., 2015). This may imply that *Beltanelliformis* had a wider environmental and/or substrate tolerance than the majority of soft-bodied Ediacaran biota.

The overlying Mooifontein Member (Zaris Formation) is composed of thin-bedded, often oolitic and intraclastic limestones that likely represent open marine subtidal deposition during the late transgression to highstand of sequence K2 (Saylor et al., 1995). The Mooifontein Member, which lacks siliciclastic interbeds above its base, is not present at either Tsaus or Grens (Fig. 6B).

5.3. Chemostratigraphic and lithostratigraphic calibration of fossil first appearances

The lithostratigraphic and sequence stratigraphic correlation presented above is supported by laterally consistent trends in $\delta^{13}C_{carb}$ between individual sections of the Witputs Sub-basin (Fig. 6B). Dominant trends in $\delta^{13}C_{carb}$ are even replicated between sections throughout the Mara Member dolostone, albeit with some scatter. The negative to positive trend in $\delta^{13}C_{carb}$ recorded through sequences K1 and K2 is a recognised time-series trend across numerous sections of the Witputs Sub-basin (Fig. 6B; Saylor et al., 1998; Hall et al., 2013), and the lower OS1 sequence of the Zaris Sub-basin, albeit with variable magnitude (e.g., Brak, Fig. S3; Wood et al., 2015). Therefore, whilst low $\delta^{13}C_{carb}$ and elevated $\delta^{18}O_{carb}$ values recorded by the Mara Member dolostone may reflect offset from open seawater composition due to deposition within a semi-restricted environment, the overall trend in $\delta^{13}C_{carb}$ throughout the Mara, Kliphoek and Aar members remains consistent with trends observed in time-equivalent regional and global datasets (Bowyer et al., 2022).

Within this framework, the oldest soft-bodied fossils of the Nama succession are found within the lower Mara Member at Tsaus, in clastics that were deposited approximately correlative to thin carbonate interbeds at Grens that record negative $\delta^{13}C_{carb}$ and elevated $\delta^{18}O_{carb}$ (Fig. 6B; Wood et al., 2015, and preprint). The lowest calibrated occurrence of skeletal *Cloudina* is also reported from the Tsaus succession, in lowstand to early transgressive carbonates that record dominantly negative $\delta^{13}C_{carb}$ and were deposited laterally equivalent to the lowstand Kliphoek quartzite (Fig. 6B). These *Cloudina* predate the 0‰ crossing point during recovery from the BANE, and are also older than the lowest documented occurrence of *Cloudina* from the Zaris Sub-basin, based on inter-basinal lithostratigraphic, $\delta^{13}C_{carb}$ chemostratigraphic and sequence stratigraphic correlation (Fig. S3; Saylor et al., 1995, 1998; Bowyer et al., 2022).

5.4. Paleoredox setting of fossil first appearances

Published regional paleoredox proxy data for the Kuibis Subgroup of the Witputs Sub-basin include Fe-speciation and rare earth element (Ce/Ce*) analyses of carbonates and shales from Grens and Arasab (Wood et al., 2015; Tostevin et al., 2016). Integration of these data shows that the environment was characterised by temporally dynamic paleoredox, dominated by anoxic ferruginous and manganous conditions, during deposition of at least the upper Mara Member, and fossiliferous Kliphoek and Aar members (Fig. 6B; Wood et al., 2015; Tostevin et al., 2016).

Due to sample averaging, bulk redox proxies integrate dominant water column redox conditions over long timescales, such that the ecological timescales of regional environmental oxygenation required for metazoan habitation are obscured (e.g., Wood et al., 2015; Sperling et al., 2016). Indeed, data suggest that *Cloudina* and other contemporary benthos in the Nama Group opportunistically colonised substrate during short-lived oxic intervals (Wood et al., 2015).

Available data do not therefore support a long-term shift towards more stable, oxygenated conditions as a driver for the first appearance of skeletonization. Rather, the combined data might support redox instability as a mechanistic driver for the generation of evolutionary novelty, followed by innovation and diversification by a number of other skeletal tubular and non-tubular animals that constitute the Nama assemblage (Figs. 1, S1, Table S1; Wood et al., 2023; Wood and Erwin, 2018).

We note, however, that the appearance of diverse metazoans in the lower Kliphoek Member coincides with a major sea-level lowstand or during very early transgression, where shallow, proximal sandstone settings supported a diverse soft-bodied biota and *Cloudina* first appeared in deeper, more distal limestones (Figs. 6, 7D). On the Siberian Platform during the Lower Cambrian, a similar relationship was found where elevated biodiversity and speciation of reef-associated sponges coincided with sea-level lowstands, which were hypothesized to represent intervals when a relative deepening of the shallow redoxcline permitted more extensive oxygenation of shallow waters over the entire craton (Zhuravlev et al., 2023). We similarly hypothesize here that, as open marine carbonate settings were required to support the calcifying *Cloudina*, it was sea level lowstands that may have enabled oxygenation of these more distal settings. Thus, expansion of shallow marine oxygen driven by sea-level oscillations may have provided an evolutionary driver for both innovations that were not highly metabolically costly such as the onset of biomineralization in *Cloudina* without strong biological control, as well as speciation events during the Ediacaran-Cambrian radiation.

6. Conclusions

The advent of animal biomineralization marks a fundamental innovation in the history of life and Earth's biogeochemical cycles. The terminal Ediacaran Nama Group, Namibia, documents the first appearance of metazoan skeletonization in the wake of a potentially significant biodiversity crisis of soft-bodied biota. However, despite its importance, the precise age and environmental context of this major evolutionary event has been poorly understood.

Here, we document the oldest occurrence of *Cloudina* from the Tsaus Mountains of the Nama Group and constrain this occurrence within a regional chemostratigraphic and paleoenvironmental context. This reveals that *Cloudina* first appeared in open marine carbonate settings, contemporaneous with the Kliphoek quartzite deposited in more proximal settings that bears diverse soft-bodied metazoans. Limestones that host *Cloudina* record negative $\delta^{13}C_{carb}$ values, that immediately precede the 0‰ crossing point during recovery from the basal Nama negative $\delta^{13}C_{carb}$ excursion. The regional environment that hosted the oldest *Cloudina* was typified by temporally dynamic, and dominantly low oxygen conditions, where metazoan habitation was facilitated during intervals of short-lived ventilation.

We conclude that the available data do not appear to support a long-term shift towards more stable, oxygenated conditions as a driver for the first appearance of skeletonization, but do suggest that distal, open marine carbonate settings were required to support the calcifying *Cloudina* which, while not under strong biological control, may have required seawater of high carbonate supersaturation. The appearance of *Cloudina* also coincided with a major sea level lowstand, which we hypothesise may have enabled oxygenation of these more distal settings. Such an expansion of shallow marine oxygen may have provided an evolutionary driver for innovations that were not metabolically costly, such as the onset of biomineralization in *Cloudina*.

Pledge

The area studied in this manuscript is a pristine nature reserve. All sampling for this study was undertaken without destructive excavation of in-situ beds. The environment was left visibly as found on arrival.

CRediT authorship contribution statement

Fred T. Bowyer: Conceptualization, Data curation, Investigation, Methodology, Project administration, Visualization, Writing – original draft, Writing – review & editing. **Collen-Issia Uahengo:** Conceptualization, Investigation, Project administration, Resources, Writing – review & editing, Methodology, Supervision. **Kavevaza Kaputuaza:** Investigation, Writing – review & editing. **Junias Ndeunyema:** Investigation, Writing – review & editing. **Mariana Yiales:** Investigation, Writing – review & editing. **Ruaridh D. Alexander:** Investigation, Writing – review & editing. **Andrew Curtis:** Investigation, Writing – review & editing. **Rachel A. Wood:** Conceptualization, Funding acquisition, Investigation, Project administration, Supervision, Writing – review & editing.

Declaration of competing interest

The authors declare that they have no known competing financial interests or personal relationships that could have appeared to influence the work reported in this paper.

Data availability

All new data are available in the supplementary material. For the purpose of open access, the authors have applied a Creative Commons Attribution (CC BY) licence to any Author Accepted Manuscript version arising.

Acknowledgements

Funding: F.B. and R.W. acknowledge funding from NERC Project NE/T008458/1. M.Y. acknowledges funding from the Beca de Doctorado en el Extranjero, Becas Chile from ANID. We thank Harry E.T. Tjihukununa of the Ministry of Environment, Forestry and Tourism, Directorate of Wildlife and National Parks for permission to access the Tsau Khaeb National Park for the purpose of research, and ranger Alex Mowe for site access. We thank U. Baranowski for technical support. F.B. thanks K.-H. Hoffmann and F. Fusseis for enlightening discussions. We thank Editor Laurence Coogan and two anonymous reviewers for thoughtful and detailed comments that greatly improved this submission.

Appendix A. Supplementary material

Supplementary material related to this article can be found online at https://doi.org/10.1016/j.epsl.2023.118336.

References

Adams, E.W., Grotzinger, J.P., Watters, W.A., Schröder, S., McCormick, D.S., Al-Siyabi, H.A., 2005. Digital characterization of thrombolite-stromatolite reef distribution in a carbonate ramp system (terminal proterozoic, Nama Group, Namibia). Am. Assoc. Pet. Geol. Bull. 89, 1293–1318.

Bengtson, S., 2004. Early skeletal fossils. In: Lipps, J.H., Waggoner, B.M. (Eds.), Neoproterozoic-Cambrian Biological Revolutions. In: The Paleontological Society Papers, pp. 67–77.

Boag, T.H., Darroch, S.A.F., Laflamme, M., 2016. Ediacaran distributions in space and time: testing assemblage concepts of earliest macroscopic body fossils. Paleobiology 42, 574–594.

Boggiani, P.C., Gaucher, C., Sial, A.N., Babinski, M., Simon, C.M., Riccomini, C., Ferreira, V.P., Fairchild, T.R., 2010. Chemostratigraphy of the Tamengo Formation (Corumbá Group, Brazil): a contribution to the calibration of the Ediacaran carbon-isotope curve. Precambrian Res. 182, 382–401.

Bowring, S.A., Grotzinger, J.P., Condon, D.J., Ramezani, J., Newall, M.J., Allen, P.A., 2007. Geochronologic constraints on the chronostratigraphic framework of the Neoproterozoic Huqf Supergroup, Sultanate of Oman. Am. J. Sci. 307, 1097–1145.

Bowyer, F.T., Zhuravlev, A.Y., Wood, R., Shields, G.A., Curtis, A., Poulton, S.W., Condon, D.J., Yang, C., Zhu, M., 2022. Calibrating the temporal and spatial dynamics of the Ediacaran-Cambrian radiation of animals. Earth-Sci. Rev. 225, 103913.

Bowyer, F.T., Zhuravlev, A.Y., Wood, R., Zhao, F., Sukhov, S.S., Alexander, R.D., Poulton, S.W., Zhu, M., 2023. Implications of an integrated late Ediacaran to early Cambrian stratigraphy of the Siberian Platform, Russia. Geol. Soc. Am. Bull. https://doi.org/10.1130/B36534.1.

Chen, Z., Zhou, C., Xiao, S., Wang, W., Guan, C., Hua, H., Yuan, X., 2014. New Ediacaran fossils preserved in marine limestone and their ecological implications. Sci. Rep. 4, 4180.
Cohen, B.L., 2005. Not armour, but biomechanics, ecological opportunity and increased fecundity as keys to the origin and expansion of the mineralized benthic metazoan fauna. Biol. J. Linn. Soc. 85, 483–490.
Cribb, A.T., Kenchington, C.G., Koester, B., Gibson, B.M., Boag, T.H., Racicot, R.A., Mocke, H., Laflamme, M., Darroch, S.A.F., 2019. Increase in metazoan ecosystem engineering prior to the Ediacaran–Cambrian boundary in the Nama Group, Namibia. R. Soc. Open Sci. 6 (9), 190548.
Darroch, S.A.F., Smith, E.F., Laflamme, M., Erwin, D.H., 2018. Ediacaran extinction and Cambrian explosion. Trends Ecol. Evol. 33, 653–663.
Degens, E.T., Kazmierczak, J., Ittekott, V., 1985. Cellular response to Ca^{2+} stress and its geological implications. Acta Palaeontol. Pol. 30, 115–135.
Dibenedetto, S., Grotzinger, J., 2005. Geomorphic evolution of a storm-dominated carbonate ramp (c. 549 Ma), Nama Group, Namibia. Geol. Mag. 142, 583–604.
Evans, S.D., Tu, C., Rizzo, A., Surprenant, R.L., Boan, P.C., McCandless, H., Marshall, N., Xiao, S., Droser, M.L., 2022. Environmental drivers of the first major animal extinction across the Ediacaran White Sea-Nama transition. Proc. Natl. Acad. Sci. USA 119, e2207475119.
Germs, G.J., 1972. New shelly fossils from the Nama Group, South-West Africa. Am. J. Sci. 272, 752–761.
Germs, G.J.B., 1974. The Nama Group in South West Africa and its relationship to the Pan-African Geosyncline. J. Geol. 82 (3), 301–317.
Germs, G.J.B., 1983. Implications of a sedimentary facies and depositional environmental analysis of the Nama Group in South West Africa/Namibia. Spec. Publ., Geol. Soc. S. Afr. 11, 89–114.
Germs, G.J.B., Gresse, P.G., 1991. The foreland basin of the Damara and Gariep orogens in Namaqualand and southern Namibia: stratigraphic correlations and basin dynamics. S. Afr. J. Geol. 94 (2), 159–169.
Germs, G.J.B., Miller, R.M.G., Frimmel, H.E., Gaucher, C., 2009. Chapter 5.4 Syn- to late-orogenic sedimentary basins of southwestern Africa. Dev. Precambrian Geol. 16, 183–203.
Gilbert, P.U.P.A., Porter, S.M., Sun, C.-Y., Xiao, S., Gibson, B.M., Shenkar, N., Knoll, A.H., 2019. Biomineralization by particle attachment in early animals. Proc. Natl. Acad. Sci. USA 116, 17659–17665.
Gilbert, P.U.P.A., Bergmann, K.D., Boekelheide, N., Tambutté, S., Mass, T., Marin, F., Adkins, J.F., Erez, J., Gilbert, B., Knutson, V., Cantine, M., Ortega-Hernández, J., Knoll, A.H., 2022. Biomineralization: integrating mechanism and evolutionary history. Sci. Adv. 8, eabl9653.
Grazhdankin, D., 2004. Patterns of distribution in the Ediacaran biotas: facies versus biogeography and evolution. Paleobiology 30 (2), 203–221.
Grotzinger, J.P., 2000. Facies and paleoenvironmental setting of Thrombolite-Stromatolite Reefs, Terminal Proterozoic Nama Group (ca. 550-543 Ma), central and southern Namibia. Commun. Geol. Surv. Namib. 12, 251–264.
Grotzinger, J.P., Bowring, S.A., Saylor, B.Z., Kaufman, A.J., 1995. Biostratigraphic and geochronological constraints on early animal evolution. Science 13, 229–272.
Gürich, G., 1930. Die bislang ältesten Spuren von Organismen in Südafrika. C. R.. In: XV Int. Geol. Congr. 1929. Pretoria, Union South Africa 2, pp. 670–680.
Hahn, G., Pflug, H.D., 1985. Polypenartige Organismen aus dem Jung-Präkambrium (Nama-Gruppe) von Namibia. Geol. Palaeontol. 19, 1–13.
Hall, M., Kaufman, A.J., Vickers-Rich, P., Ivantsov, A., Trusler, P., Linnemann, U., Hofmann, M., Elliott, D., Cui, H., Fedonkin, M., Hoffmann, K.H., Wilson, S.A., Schneider, G., Smith, J., 2013. Stratigraphy, palaeontology and geochemistry of the late Neoproterozoic Aar Member, southwest Namibia: Reflecting environmental controls on Ediacara fossil preservation during the terminal Proterozoic in African Gondwana. Precambrian Res. 238, 214–232.
Kaufman, A.J., Hayes, J.M., Knoll, A.H., Germs, G.J.B., 1991. Isotopic compositions of carbonates and organic carbon from upper Proterozoic successions in Namibia: stratigraphic variation and the effects of diagenesis and metamorphism. Precambrian Res. 49, 301–327.
Knoll, A.H., 2003. Biomineralization and evolutionary history. Rev. Mineral. Geochem. 54, 329–356.
Linnemann, U., Ovtcharova, M., Schaltegger, U., Gärtner, A., Hautmann, M., Geyer, G., Vickers-Rich, P., Rich, T., Plessen, B., Hofmann, M., Zieger, J., Krause, R., Kriesfeld, L., Smith, J., 2019. New high-resolution age data from the Ediacaran–Cambrian boundary indicate rapid, ecologically driven onset of the Cambrian explosion. Terra Nova 31, 49–58.
Lowenstam, H.A., Margulis, L., 1980. Evolutionary prerequisites for early Phanerozoic calcareous skeletons. Biosystems 12, 27–41.
Muscente, A.D., Bykova, N., Boag, T.H., Buatois, L.A., Mángano, M.G., Eleish, A., Prabhu, A., Pan, F., Meyer, M.B., Schiffbauer, J.D., Fox, P., Hazen, R.M., Knoll, A.H., 2019. Ediacaran biozones identified with network analysis provide evidence for pulsed extinctions of early complex life. Nat. Commun. 10, 1–15.
Nelson, L.L., Ramezani, J., Almond, J.E., Darroch, S.A.F., Taylor, W.L., Brenner, D.C., Furey, R.P., Turner, M., Smith, E.F., 2022. Pushing the boundary: a calibrated Ediacaran-Cambrian stratigraphic record from the Nama Group in northwestern Republic of South Africa. Earth Planet. Sci. Lett. 580, 117396.
Nelson, L.L., Crowley, J.L., Smith, E.F., Schwartz, D.M., Hodgin, E.B., Schmitz, M.D., 2023. Cambrian explosion condensed: high-precision geochronology of the lower Wood Canyon Formation, Nevada. Proc. Natl. Acad. Sci. USA 120 (3), e2301478120.
Parry, L.A., Boggiani, P.C., Condon, D.J., Garwood, R.J., Leme, J.D.M., McIlroy, D., Brasier, M.D., Trindade, R., Campanha, G.A.C., Pacheco, M.L.A.F., Diniz, C.Q.C., Liu, A.G., 2017. Ichnological evidence for meiofaunal bilaterians from the terminal Ediacaran and earliest Cambrian of Brazil. Nat. Ecol. Evol. 1, 1455–1464.
Pflug, H.D., 1966. Neue Fossilreste aus den Nama-Schichten in Südwest-Afrika. Paläontol. Z. 40, 14–25.
Saylor, B.Z., Grotzinger, J.P., Germs, G.J.B., 1995. Sequence stratigraphy and sedimentology of the Neoproterozoic Kuibis and Schwarzrand Subgroups (Nama Group), southwestern Namibia. Precambrian Res. 73, 153–171.
Saylor, B.Z., Kaufman, A.J., Grotzinger, J.P., Urban, F., 1998. A composite reference section for terminal Proterozoic strata of southern Namibia. J. Sediment. Res. 68, 1223–1235.
Schiffbauer, J.D., Selly, T., Jacquet, S.M., Merz, R.A., Nelson, L.L., Strange, M.A., Cai, Y., Smith, E.F., 2020. Discovery of bilaterian-type through-guts in cloudinomorphs from the terminal Ediacaran Period. Nat. Commun. 11, 1–12.
Shore, A., Wood, R., 2021. Environmental and diagenetic controls on the morphology and calcification of the Ediacaran metazoan *Cloudina*. Sci. Rep. 11, 1–13.
Smith, E.F., Nelson, L.L., Tweedt, S.M., Zeng, H., Workman, J.B., 2017. A cosmopolitan late ediacaran biotic assemblage: new fossils from Nevada and Namibia support a global biostratigraphic link. Proc. R. Soc. B, Biol. Sci. 284, 20170934.
Smith, O., 1999. Terminal Proterozoic Carbonate Platform Development: Stratigraphy and Sedimentology of the Kuibis Subgroup (ca. 550–548 Ma), Northern Nama Basin, Namibia. Unpublished Masters Thesis. Massachusetts Institute of Technology.
Sperling, E.A., Carbone, C., Strauss, J.V., Johnston, D.T., Narbonne, G.M., Macdonald, F.A., 2016. Oxygen, facies, and secular controls on the appearance of Cryogenian and Ediacaran body and trace fossils in the Mackenzie Mountains of northwestern Canada. Bull. Geol. Soc. Am. 128, 558–575.
Topper, T., Betts, M.J., Dorjnamjaa, D., Li, G., Li, L., Altanshagai, G., Enkhbaatar, B., Skovsted, C.B., 2022. Locating the BACE of the Cambrian: Bayan Gol in southwestern Mongolia and global correlation of the Ediacaran-Cambrian boundary. Earth-Sci. Rev. 229, 104017.
Tostevin, R., Wood, R.A., Shields, G.A., Poulton, S.W., Guilbaud, R., Bowyer, F., Penny, A.M., He, T., Curtis, A., Hoffmann, K.H., Clarkson, M.O., 2016. Low-oxygen waters limited habitable space for early animals. Nat. Commun. 7, 12818.
Vermeij, G.J., 1990. The origin of skeletons. Palaios 4, 585–589.
Vickers-Rich, P., Ivantsov, A.Y., Trusler, P.W., Narbonne, G.M., Hall, M., Wilson, S.A., Greentree, C., Fedonkin, M.A., Elliott, D.A., Hoffmann, K.H., Schneider, G.I.C., 2013. Reconstructing *Rangea*: new discoveries from the Ediacaran of southern Namibia. J. Paleontol. 87, 1–15.
Waggoner, B., 2003. The Ediacaran biotas in space and time. Integr. Comp. Biol. 43, 104–113.
Wood, R., Erwin, D.H., 2018. Innovation not recovery: dynamic redox promotes metazoan radiations. Biol. Rev. 93, 863–873.
Wood, R., Bowyer, F.T., Alexander, R., Yilales, M., Uahengo, C.-I., Kaputuaza, K., Ndeunyema, J., Curtis, A., 2023. New Ediacaran biota from the oldest Nama Group, Namibia (Tsaus Mountains), and re-definition of the Nama Assemblage. (preprint) EarthArXiv. https://doi.org/10.31223/X5895W.
Wood, R.A., Poulton, S.W., Prave, A.R., Hoffmann, K.H., Clarkson, M.O., Guilbaud, R., Lyne, J.W., Tostevin, R., Bowyer, F., Penny, A.M., Curtis, A., Kasemann, S.A., 2015. Dynamic redox conditions control late Ediacaran metazoan ecosystems in the Nama Group, Namibia. Precambrian Res. 261, 252–271.
Wood, R.A., Ivantsov, A.Y., Zhuravlev, A.Y., 2017. First macrobiota biomineralization was environmentally triggered. Proc. R. Soc. B, Biol. Sci. 284, 20170059.
Xiao, S., Chen, Z., Pang, K., Zhou, C., Yuan, X., 2020. The Shibantan Lagerstätte: insights into the Proterozoic-Phanerozoic transition. J. Geol. Soc. (Lond.) 178, jgs2020-135.
Yang, B., Steiner, M., Zhu, M., Li, G., Liu, J., Liu, P., 2016. Transitional Ediacaran–Cambrian small skeletal fossil assemblages from South China and Kazakhstan: implications for chronostratigraphy and metazoan evolution. Precambrian Res. 285, 202–215.
Yang, B., Steiner, M., Schiffbauer, J.D., Selly, T., Wu, X., Zhang, C., Liu, P., 2020. Ultrastructure of Ediacaran cloudinids suggests diverse taphonomic histories and affinities with non-biomineralized annelids. Sci. Rep. 10, 1–12.
Yang, C., Rooney, A.D., Condon, D.J., Li, X.-H., Grazhdankin, D.V., Bowyer, F.T., Hu, C., Macdonald, F., Zhu, M., 2021. The tempo of Ediacaran evolution. Sci. Adv. 7, eabi9643.
Zhuravlev, A.Y., Liñán, E., Vintaned, J.A.G., Debrenne, F., Fedorov, A.B., 2012. New finds of skeletal fossils in the terminal Neoproterozoic of the Siberian Platform and Spain. Acta Palaeontol. Pol. 57, 205–224.
Zhuravlev, A.Y., Wood, R.A., Bowyer, F.T., 2023. Cambrian radiation speciation events driven by sea level and redoxcline changes on the Siberian Craton. Sci. Adv. 9, eadh2558.